6th European Conference on Computational Mechanics (ECCM 6)
7th European Conference on Computational Fluid Dynamics (ECFD 7)
11-15 June 2018, Glasgow, UK

A MIXED-MODE COHESIVE MODEL ACCOUNTING FOR SMALL TO LARGE OPENINGS TRANSITION

FEDERICA CONFALONIERI[1] AND UMBERTO PEREGO[2]

[1] University of Pavia
via Ferrata 3, 27100 Pavia, Italy
federica.confalonieri@unipv.it

[2] Politecnico di Milano
piazza Leonardo da Vinci 32, 20133 Milano, Italy
umberto.perego@polimi.it

Key words: Mixed-mode delamination, Large openings, Cohesive model. Fiber bridging

Abstract. This work addresses the formulation of a new mixed-mode cohesive model, able to handle the transition from small to large openings: the proposed model is an extension of the isotropic damage model formulated in [Confalonieri and Perego, JSSCM, 11-2, 2017] for the simulation of mixed-mode delamination with variable mode-ratio, under the assumption of small relative displacements.

1 INTRODUCTION

Delamination, often characterized by mixed-mode loading conditions with variable mode-ratio, is among the most frequent failure mechanisms in laminated composite materials, due to their low strength along inter-layer interfaces. The computational strategies for the numerical simulation of the delamination process often rely on the use of interface elements based on the cohesive zone approach. While in the case of small failure openings the interface behaviour is governed by the interaction between normal and shear tractions, when large openings are involved at complete failure, other phenomena, such as fiber bridging or interfacial fibrillation, affect the mechanical response and have to be properly accounted for in the numerical modelling. Classical cohesive models, formulated under the hypothesis of small openings, indeed fail to predict the delamination growth either in the presence of extensive fiber-bridging phenomena or when large relative displacements are involved. As shown by a number of DCB tests performed on fiber-reinforced composites, the development of large-scale fiber bridging causes an increment in the fracture energy [1, 2, 3]. This effect, mainly governed by the normal opening, is typically described in terms of R-curves, expressing the progressive growth of the toughness up to a steady-state value as a function of the crack extension. Furthermore, in the presence of large openings, the rotational equilibrium of the cohesive element may not be satisfied by classical cohesive approaches, as discussed in [4, 5].

In this work the isotropic damage cohesive model formulated in [6] under the assumption of small openings is extended to properly model both the cases of small and large openings and the presence of large-scale bridging. The considered cohesive model is specifically conceived for the case of mixed-mode delamination with variable mode-ratios and is used to handle the small opening case. Consistent with the fact that fiber bridging and fibrillation are mainly driven by Mode I loading conditions, two different traction-separation laws are considered in pure Mode I and II. A classical bilinear traction separation law is adopted in pure Mode II. The traction separation law in pure Mode I is, instead, characterized by a trilinear softening branch, as it has been proposed in [7, 8, 9]. A fibril element, inspired to the directional cohesive element described in [10, 11] and conceptually similar to the cohesive zone model proposed in [12], is adopted to account for large openings, ensuring rotational equilibrium since the interface tractions and openings are co-linear. In pure Mode I, it is assumed that the transition from the small openings continuum model to the fibril one takes place at the damage level corresponding to the change of slope in the softening branch. In mixed-mode, the transition is assumed to be triggered at a damage level increasing with the mode-ratio, whereas no transition can occur in Mode II. The insertion of the fibril element is smooth, with no discontinuities in the dissipated energy, nor in the transmitted cohesive tractions.

In section 2, the damage cohesive model developed for mixed-mode delamiantion under small relative displacements is briefly recalled and its formulation is generalized to the case of different shapes of the traction-separation law in mode I and II. In section 3 the procedure for the transition from the small openings model to the large openings one is described. In section 4, the fibril element model adopted for the large displacement case is described.

2 SMALL OPENINGS MODEL

2.1 Isotropic damage cohesive model

The small opening case is handled by means of a classical cohesive interface element. Let us consider a cohesive zero-thickness interface Γ separating two adjacent material layers: the two sides of the interface after separation are denoted as Γ^+ and Γ^-. Let $\boldsymbol{\delta} = [\delta^n \ \delta^s]^T$ denote the vector of the small relative displacement between two initially coincident points, belonging to the two displaced sides, and let $\mathbf{t} = [t^n \ t^s]^T$ be the vector of the tractions exchanged between the two sides at the same point: t^n and δ^n represent the components of tractions and openings normal to the initial interface Γ, while t^s and δ^s are the tangential components in the local orthogonal reference frame. Under the assumption of small displacements, the interface local reference frame is uniquely defined by the initial interface configuration. The isotropic damage cohesive model proposed in [6] for the simulation of mixed-mode delamination problems, whose formulation is recalled hereafter, is adopted to describe the interface constitutive behaviour. Only the case of mixed-mode delamination is considered in this work: isotropic properties in the interface tangent plane (transverse isotropy) are therefore assumed.

The starting point in the formulation of the cohesive model is the definition of the free

energy potential Ψ per unit surface:

$$\Psi = \frac{1}{2}K\left(\langle\delta^n\rangle_-\right)^2 + \frac{1}{2}\left(1-d\right)K\left(\langle\delta^n\rangle_+\right)^2 + \frac{1}{2}\left(1-d\right)K(\delta^s)^2 \tag{1}$$

being d an isotropic damage variable and K the stiffness paramater, defining the initial elastic response and assumed equal in all directions. The Macauley brackets $\langle\ \rangle$ are introduced to account for the unilateral effect and to prevent interpenetration upon interface closure. The cohesive tractions t^n, t^s and the strain energy release rate Y per unit damage growth are obtained through the state equations:

$$t^n = \frac{\partial\Psi}{\partial\delta^n} = K\langle\delta^n\rangle_- + \left(1-d\right)K\langle\delta^n\rangle_+, \quad t^s = \frac{\partial\Psi}{\partial\delta^s} = \left(1-d\right)K\delta^s \tag{2}$$

$$Y = -\frac{\partial\Psi}{\partial d} = \frac{1}{2}K\left(\langle\delta^n\rangle_+\right)^2 + \frac{1}{2}K\left(\delta^s\right)^2 \tag{3}$$

Let us introduce the vectors of non-dimensional tractions and separations obtained by normalizing with respect to the elastic threshold values in the pure modes. t_0^I, t_0^{II}, δ_0^I and δ_0^{II} as:

$$\bar{\mathbf{t}} = \begin{Bmatrix} \frac{t^n}{t_0^I} \\ \frac{t^s}{t_0^{II}} \end{Bmatrix} = \begin{Bmatrix} \bar{t}^n \\ \bar{t}^s \end{Bmatrix} \quad \bar{\boldsymbol{\delta}} = \begin{Bmatrix} \frac{\delta^n}{\delta_0^I} \\ \frac{\delta^s}{\delta_0^{II}} \end{Bmatrix} = \begin{Bmatrix} \bar{\delta}^n \\ \bar{\delta}^s \end{Bmatrix} \tag{4}$$

For the sake of simplicity, only the tensile case will be addressed in the following. The relation between non-dimensional tractions and opening displacements in the damage range is therefore given by:

$$\bar{t}^n = \left(1-d\right)\bar{\delta}^n, \quad \bar{t}^s = \left(1-d\right)\bar{\delta}^s \tag{5}$$

The interaction between normal and shear interlaminar stresses is accounted for by introducing a damage activation locus in the non-dimensional traction components plane. Focusing on the tensile side of the non-dimensional tractions plane, three different damage modes, whose combination determines the shape of the activation locus, are identified as shown in Figure 1): a normal opening mode, associated to mode I delamination and characterized by the normal $\mathbf{n}^1$; two mixed-mode mechanisms, one for positive and one for negative shear, characterized by the normals $\mathbf{n}^2$ and $\mathbf{n}^3$ to two planes, inclined by angles α and $-\alpha$ with respect to the t^n axis. The angle α plays the role of a constitutive parameter for the proposed model.

$$\mathbf{n}^1 = \begin{Bmatrix} 1 \\ 0 \end{Bmatrix}, \quad \mathbf{n}^2 = \begin{Bmatrix} \sin\alpha \\ \cos\alpha \end{Bmatrix}, \quad \mathbf{n}^3 = \begin{Bmatrix} \sin\alpha \\ -\cos\alpha \end{Bmatrix} \tag{6}$$

The effective tractions $\mathbf{s} = \{s^1\ s^2\ s^3\}^T$ obtained by projecting the traction vector onto the damage modes are introduce to measure the distance of the current traction vector from the activation locus:

$$\begin{aligned} s^1 &= \bar{\mathbf{t}}\cdot\mathbf{n}^1 = \bar{t}^n \\ s^2 &= \bar{\mathbf{t}}\cdot\mathbf{n}^2 = \bar{t}^n\sin\alpha + \bar{t}^s\cos\alpha \\ s^3 &= \bar{\mathbf{t}}\cdot\mathbf{n}^3 = \bar{t}^n\sin\alpha - \bar{t}^s\cos\alpha \end{aligned} \tag{7}$$

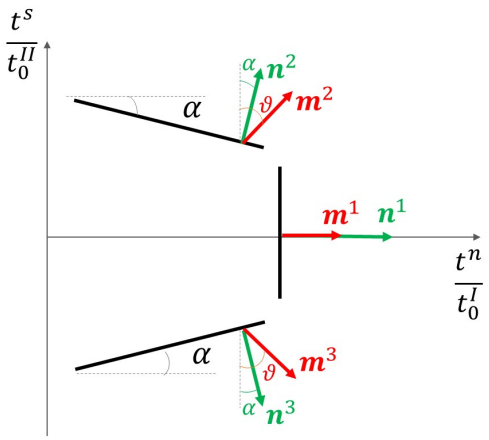

Figure 1: Activation domain: main damage modes

In a similar way, one can also define effective openings w^1, w^2, w^3, conjugate to the effective tractions, by projecting the interface opening displacements onto the directions defined by a set of three structural vectors $\mathbf{m}^1$, $\mathbf{m}^2$, $\mathbf{m}^3$ depending on an angle θ (Figure 1), with:

$$\mathbf{m}^1 = a\mathbf{n}^1 = \begin{Bmatrix} a \\ 0 \end{Bmatrix}, \quad \mathbf{m}^2 = b \begin{Bmatrix} \sin\theta \\ \cos\theta \end{Bmatrix}, \quad \mathbf{m}^3 = b \begin{Bmatrix} \sin\theta \\ -\cos\theta \end{Bmatrix} \tag{8}$$

and

$$\begin{aligned} w^1 &= \bar{\delta} \cdot \mathbf{m}^1 = a\bar{\delta}^n \\ w^2 &= \bar{\delta} \cdot \mathbf{m}^2 = b\left[\bar{\delta}^n \sin\theta + \bar{\delta}^s \cos\theta\right] \\ w^3 &= \bar{\delta} \cdot \mathbf{m}^3 = b\left[\bar{\delta}^n \sin\theta - \bar{\delta}^s \cos\theta\right] \end{aligned} \tag{9}$$

The constants a and b, governing the magnitude of the structural vectors, can be determined by enforcing the following energy equivalence:

$$\Psi = \frac{1}{2}\mathbf{t} \cdot \delta = \frac{1}{2}\left(t_0^I \delta_0^I \bar{t}^n \bar{\delta}^n + t_0^{II}\delta_0^{II} + \bar{t}^s \bar{\delta}^s\right) = \underbrace{\frac{1}{2}s^1 w^1}_{\Psi^1} + \underbrace{\frac{1}{2}s^2 w^2}_{\Psi^2} + \underbrace{\frac{1}{2}s^3 w^3}_{\Psi^3} \tag{10}$$

obtaining

$$a = \left(t_0^I \delta_0^I - t_0^{II}\delta_0^{II} \tan\alpha \tan\theta\right), \qquad b = \frac{t_0^{II}\delta_0^{II}}{2\cos\alpha\cos\theta} \tag{11}$$

The projection of the interface tractions and openings onto the three damage modes allows in a straightforward way for an additive decomposition of the free energy into three contributions associated to the damage modes (eqn. (10)). The driving forces individually acting on each one of the damage modes and promoting damage growth can be obtained through the state equations. If, in addition, one sets

$$\theta = \arctan\left(\frac{t_0^I \delta_0^I}{t_0^{II}\delta_0^{II}} \tan\alpha\right) \tag{12}$$

one has:

$$
\begin{aligned}
Y^1 &= -\frac{\partial \Psi^1}{\partial d} = \frac{1}{2} t_0^I \delta_0^I \left(1 - \tan^2 \alpha\right) \left(\overline{\delta}^n\right)^2 \\
Y^2 &= -\frac{\partial \Psi^2}{\partial d} = \frac{1}{4} \left(\tan \alpha \, \overline{\delta}^n + \overline{\delta}^s\right) \left(t_0^I \delta_0^I \tan \alpha \, \bar{\delta}^n + t_0^{II} \delta_0^{II} \, \bar{\delta}^s\right) \\
Y^3 &= -\frac{\partial \Psi^3}{\partial d} = \frac{1}{4} \left(\tan \alpha \, \bar{\delta}^n - \bar{\delta}^s\right) \left(t_0^I \delta_0^I \tan \alpha \, \bar{\delta}^n - t_0^{II} \delta_0^{II} \, \bar{\delta}^s\right)
\end{aligned}
\tag{13}
$$

so that $Y^1 \geq 0$ for $\alpha < 45°$; moreover, also the sum $Y^2 + Y^3$, representing the fraction of the strain energy release rate associated to the shear-dominated damage modes, is always non-negative, while either Y^2 or Y^3 can be negative. It holds that:

$$
Y^1 + Y^2 + Y^3 = \frac{1}{2} t_0^I \delta_0^I \left(\overline{\delta}^n\right)^2 + \frac{1}{2} t_0^{II} \delta_0^{II} \left(\overline{\delta}^s\right)^2 = Y \geq 0 \quad \forall \overline{\delta}^n, \overline{\delta}^s \tag{14}
$$

The energy decomposition in (10) naturally leads to the definition of an energy threshold associated to each damage mode and to the formulation of a damage activation function φ, where each driving force is compared to the current value of its threshold:

$$
\varphi = \left(\frac{Y^1}{\chi_0^1 + \chi^1(d)}\right)^k + H(Y^2) \left(\frac{Y^2}{\chi_0^2 + \chi^2(d)}\right)^k + H(Y^3) \left(\frac{Y^3}{\chi_0^3 + \chi^3(d)}\right)^k - 1 \leq 0 \tag{15}
$$

where the exponent k is a parameter of the model, $H()$ is the Heaviside function, introduced to avoid possible negative contributions of Y^2 and Y^3 to damage activation, and $\chi^i + \chi_0^i$ is the current threshold for the i-th damage mode, evolving during the decohesion process as a function of the damage variable d. $\chi_0^i > 0$ represents the initial threshold, while $\chi^i(d) \geq 0$ is the internal variable, governing the threshold evolution for increasing damage and determining the shape of the softening branch. Damage evolution is obtained in a classical way enforcing the conditions $\varphi = 0$ and $\dot{\varphi} = 0$. The formulation of the cohesive model is completed by the introduction of the following loading-unloading conditions:

$$
\varphi \leq 0, \qquad \dot{d} \geq 0, \qquad \varphi \dot{d} = 0 \tag{16}
$$

2.2 Traction-separation laws

Two distinct forms of the traction-separation law, different in Mode I and II, are considered in this work to account for the fact that fiber bridging is promoted mainly by Mode I loading conditions: a classical bilinear law in Mode II and a trilinear law in Mode I (see Figure 2). The resulting mixed-mode response is shown in Figure 3.

Since the internal variables $\chi^i(d)$ govern the shape of the softening branches, their analytical expressions can be obtained by considering pure Mode I and II loading conditions, i.e by imposing that:

$$
\delta^n \neq 0 \quad \delta^s = 0 \qquad \text{for pure mode I} \tag{17}
$$

$$
\delta^n = 0 \quad \delta^s \neq 0 \qquad \text{for pure mode II} \tag{18}
$$

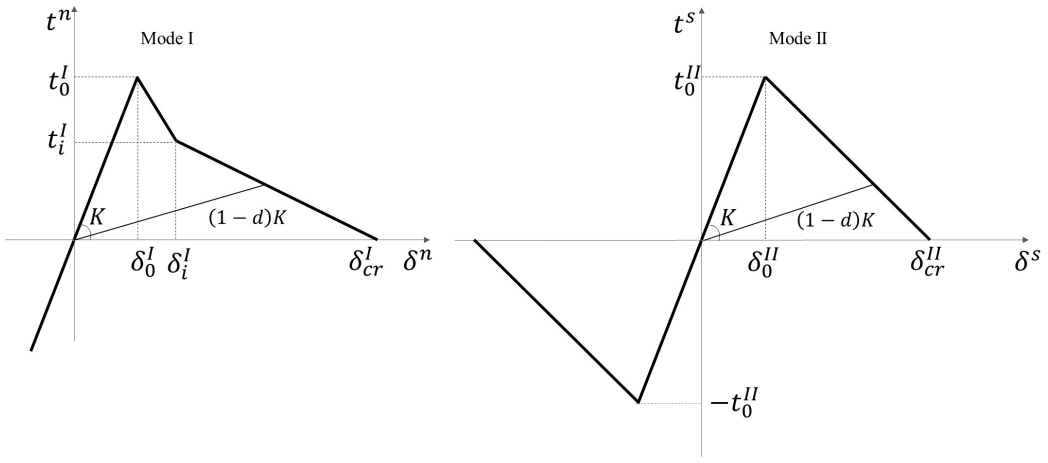

Figure 2: Traction-separation laws in pure modes I and II.

In the case of pure mode loading paths, the relationships between the isotropic damage and the opening displacements can be established on the basis of purely geometric considerations. The pure mode I traction-separation law can be described as:

$$t^n = \frac{t_0^I}{\delta_0^I}\delta^n \qquad \text{for} \quad \delta^n \leq \delta_0^I \tag{19}$$

$$t^n = (1-d)\,\frac{t_0^I}{\delta_0^I}\delta^n = t_i^I + \left(t_0^I - t_i^I\right)\frac{\delta_i^I - \delta^n}{\delta_i^I - \delta_0^I} \qquad \text{for} \quad \delta_0^I \leq \delta^n \leq \delta_i^I \tag{20}$$

$$t^n = (1-d)\,\frac{t_0^I}{\delta_0^I}\delta^n = t_i^I\frac{\delta_{cr}^I - \delta^n}{\delta_{cr}^I - \delta_i^I} \qquad \text{for} \quad \delta_i^I \leq \delta^n \leq \delta_{cr}^I \tag{21}$$

where the symbols are defined in Figure 2. From (20) and (21), it is possibile to derive the expression of the relative displacement δ^n as a function of the damage variable d for the two softening branches:

$$\delta^n = \delta_0^I\frac{\left(t_0^I\delta_i^I - t_i^I\delta_0^I\right)}{\left(t_0^I\delta_i^I - t_i^I\delta_0^I\right) - dt_0^I\left(\delta_i^I - \delta_0^I\right)} \qquad \text{for} \quad \delta_0^I \leq \delta^n \leq \delta_i^I \tag{22}$$

$$\delta^n = \delta_0^I\frac{t_i^I\delta_{cr}^I}{(1-d)\,t_0^I\left(\delta_{cr}^I - \delta_i^I\right) + t_i^I\delta_0^I} \qquad \text{for} \quad \delta_i^I \leq \delta^n \leq \delta_{cr}^I \tag{23}$$

Similarly, in pure mode II loading, it holds that:

$$t^s = \frac{t_0^{II}}{\delta_0^{II}}\delta^s \qquad \text{for} \quad \delta^s \leq \delta_0^{II} \tag{24}$$

$$t^s = (1-d)\,\frac{t_0^{II}}{\delta_0^{II}}\delta^s = t_0^{II}\frac{\delta_{cr}^{II} - \delta^s}{\delta_{cr}^{II} - \delta_0^{II}} \qquad \text{for} \quad \delta_0^{II} \leq \delta^s \leq \delta_{cr}^{II} \tag{25}$$

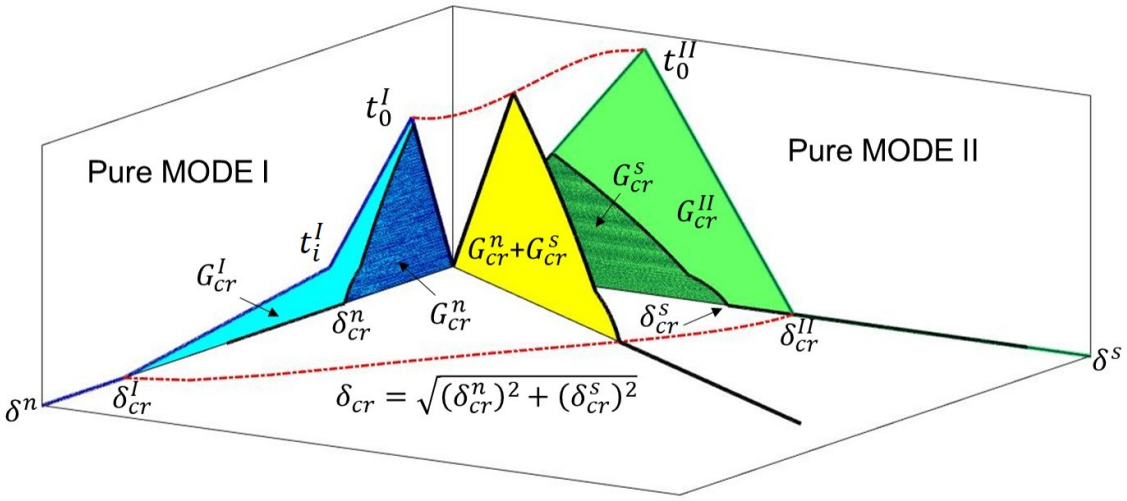

Figure 3: Mixed-mode traction-separation law for varying mode-ratio.

thus, from equation (25):

$$\delta^s = \frac{\delta_{cr}^{II}\delta_0^{II}}{\delta_{cr}^{II} - (\delta_{cr}^{II} - \delta_0^{II})d} \qquad \text{for} \quad \delta_0^{II} \leq \delta^s \leq \delta_{cr}^{II} \tag{26}$$

The effective strain energy release rates per unit of damage growth under pure mode I and II loading conditions can be found by substituting (17) and (18) into (13):

$$Y^{1,I} = \tfrac{1}{2} t_0^I \delta_0^I \left(1 - \tan^2\alpha\right) \left(\overline{\delta}^n\right)^2 \qquad Y^{1,II} = 0 \tag{27}$$

$$Y^{2,I} = \tfrac{1}{4} t_0^I \delta_0^I \tan^2\alpha \left(\overline{\delta}^n\right)^2 \qquad Y^{2,II} = \frac{1}{4} t_0^{II} \delta_0^{II} \left(\overline{\delta}^s\right)^2 \tag{28}$$

$$Y^{3,I} = \tfrac{1}{4} t_0^I \delta_0^I \tan^2\alpha \left(\overline{\delta}^n\right)^2 \qquad Y^{3,II} = \frac{1}{4} t_0^{II} \delta_0^{II} \left(\overline{\delta}^s\right)^2 \tag{29}$$

where $Y^{i,I}$ and $Y^{i,II}$ are the driving forces for pure mode I and mode II loading conditions, respectively.

Since the behavior in pure mode II in (27)–(29) is uncoupled, i.e. a sliding displacement $\bar{\delta}^s$ produces a zero driving force $Y^{1,II}$, associated to the normal opening damage mechanism 1 in Figure 1, while $Y^{2,I} \neq 0$ and $Y^{3,I} \neq 0$ in pure mode I, it is necessary to first define $\chi^2(d)$ and $\chi^3(d)$ in the pure mode II case and, then, define $\chi^1(d)$ in the pure mode I case on the basis on the results obtained for mode II. For both pure mode loading conditions, the expression of the initial thresholds χ_0^i can be determined by imposing that the activation criterion is fulfilled at the onset of delamination, i.e. $\varphi = 0$ for $d = 0$ and

$\overline{\delta}^m = 1$ with $m = n$ in pure mode I and $m = s$ in pure mode II:

$$\chi_0^1 = \frac{1}{2}\frac{t_0^I \delta_0^I \left(1 - \tan^2\alpha\right)}{\left[1 - \left(\frac{t_0^I \delta_0^I}{t_0^{II}\delta_0^{II}}\tan^2\alpha\right)^k\right]^{\frac{1}{k}}} \qquad \chi_0^2 = \chi_0^3 = 2^{\frac{1}{k}}\frac{1}{4}t_0^{II}\delta_0^{II} \tag{30}$$

Similarly, the expressions of the internal variables χ^i can be found by imposing that the activation criterion is met for $d > 0$ and $\overline{\delta}^m > 1$.

$$\chi^2(d) = \chi^3(d) = 2^{\frac{1}{k}}\frac{1}{4}t_0^{II}\delta_0^{II}\left[\frac{\delta_{cr}^{II}}{\delta_{cr}^{II} - \left(\delta_{cr}^{II} - \delta_0^{II}\right)d}\right]^2 - \chi_0^2 \tag{31}$$

$$\chi^1(d) = \frac{t_0^I \delta_0^I \left(1 - \tan^2\alpha\right)\left(\bar{x}^1\right)^2}{\left\{1 - \left[\left(\bar{x}^1\right)^2\left(\frac{\delta_{cr}^{II} - \left(\delta_{cr}^{II} - \delta_0^{II}\right)d}{\delta_{cr}^{II}}\right)^2 \frac{t_0^I\delta_0^I}{t_0^{II}\delta_0^{II}}\tan^2\alpha\right]^k\right\}^{\frac{1}{k}}} - \chi_0^1 \tag{32}$$

being

$$\bar{x}^1 = \frac{t_0^I\delta_i^I - t_i^I\delta_0^I}{\left(t_0^I\delta_i^I - t_i^I\delta_0^I\right) - dt_0^I\left(\delta_i^I - \delta_0^I\right)} \qquad \text{for} \quad \delta_0^I \le \delta^n \le \delta_i^I \tag{33}$$

$$\bar{x}^1 = \frac{t_i^I\delta_{cr}^I}{\left(1-d\right)t_0^I\left(\delta_{cr}^I - \delta_i^I\right) + t_i^I\delta_0^I} \qquad \text{for} \quad \delta_i^I \le \delta^n \le \delta_{cr}^I \tag{34}$$

3 TRANSITION FROM SMALL TO LARGE OPENINGS

The transition from small to large openings is here modelled substituing the classical interface element with a fibril element, whose model will be described in section 4. A mixed-mode fibril insertion criterion is formulated assuming that, as in [8], the development of fiber bridging in pure Mode I occurs in correspondence of the change in slope of the softening branch of the Mode I traction-separation law and that in mixed-mode conditions, the transition has to be activated for a damage level progressively increasing with the mode-ratio from a minimum δ_i^I in Mode I to 1 in Mode II (i.e. no transition occurs in pure Mode II). The fiber activation criterion is written comparing the energy G^1 dissipated by Y^1, i.e. by the driving force associated to the opening damage mode, with an energy threshold G_i^I defined as the energy dissipated by the driving force $Y^{1,I}$ (see eqn. 27) in reaching the damage level d_i^I corresponding to the change of slope in the softening branch along a pure Mode I loading path:

$$G^1 = \int_0^{d_i} Y^1 \dot{d} \ge G_i^I = \int_0^{d_i^I} Y^{1,I}\dot{d} \tag{35}$$

where d_i is the damage corresponding to the fiber activation in mixed-mode conditions. Once the criterion is fulfilled, the classical interface element is substituted with a fibril element, without introducing any discontinuity in the transmitted tractions and in the remaining energy to be dissipated.

4 FIBRIL ELEMENT

The large opening formulation is based on the use of a directional (or fibril) cohesive element [10, 11], shown in Figure 4a, which connects along a straight line two points belonging to the interface flanks and coincident in the undeformed configuration. This kind of element provides co-linear interface tractions and openings, since the cohesive forces $\mathbf{T}^+$ and $\mathbf{T}^-$ are transmitted along the direction of the fibril and is therefore able to account for large openings in a consistent way, as discussed in [4]. The fibril element has a non-zero initial length, given by the distance between the two points on the two sides of the interface, measured at the fibril insertion. A rigid softening cohesive model with linear softening branch, depicted in Figure 4b, links the magnitude T of the cohesive force transmitted by the fibril element to its elongation Δl, computed as the difference between the length of the fibril in the current configuration and its initial length. The cohesive law can be described by means of the following set of equations:

$$T = T_0 \frac{\Delta l_{cr} - \Delta l}{\Delta l_{cr}} \quad \text{for } \Delta l \geq \Delta \bar{l} \qquad \text{loading} \tag{36}$$

$$T = T_0 \frac{\Delta l_{cr} - \Delta \bar{l}}{\Delta l_{cr}} \frac{\Delta l}{\Delta \bar{l}} \quad \text{for } \Delta l < \Delta \bar{l} \qquad \text{unloading} \tag{37}$$

$$T = 0 \qquad \text{for } \Delta l \geq \Delta l_{cr} \qquad \text{complete decohesion} \tag{38}$$

where T_0 is the fibril initial cohesive traction, computed as the modulus of the traction vector at fibril insertion, $\Delta \bar{l}$ is the maximum relative elongation, which works as the historical variable and allows to distinguish between the loading and unloading phases, and Δl_{cr} represents the critical fibril length corresponding to the ultimate opening. The area beneath the curve represents the energy that remains to be dissipated by the fibril before it reaches its critical elongation. To guarantee a smooth transition from the small openings model to the large openings one, this energy is assumed to be equal to the difference between the energy dissipation at failure due to $Y^{1,I}$ in pure mode I and G_i^I. The cohesive tractions transmitted by a single fibril element are, thus, given by:

$$\mathbf{T}^+ = T\mathbf{v}^+ \qquad \mathbf{T}^- = T\mathbf{v}^- \tag{39}$$

where the unit vectors $\mathbf{v}^+$ and $\mathbf{v}^-$ are defined as:

$$\mathbf{v}^+ = -\mathbf{v}^- = \frac{\mathbf{x}^+ - \mathbf{x}^-}{\|\mathbf{x}^+ - \mathbf{x}^-\|} = \frac{l}{\|\mathbf{x}^+ - \mathbf{x}^-\|} \tag{40}$$

being $\mathbf{x}^+$ and $\mathbf{x}^-$ the spatial coordinates of the two string nodes attached to the interface flanks Γ^+ and Γ^- respectively.

5 NUMERICAL EXAMPLES

The proposed transition procedure is assessed with reference to the a simple numerical test on a single interface element, similar to the one proposed in [5]. Let us consider the 4-node interface element with two Gauss points shown in Figure 5a, whose bottom nodes are held fixed, while the upper nodes are subjected to two distinct displacement vectors, such that $U^x_{1^+} = \bar{U} f(t) \quad U^y_{1^+} = \bar{V} f(t) \quad U^x_{2^+} = c_U \bar{U} f(t) \quad U^y_{2^+} = c_V \bar{V} f(t)$, being $\bar{U}(t)$ and

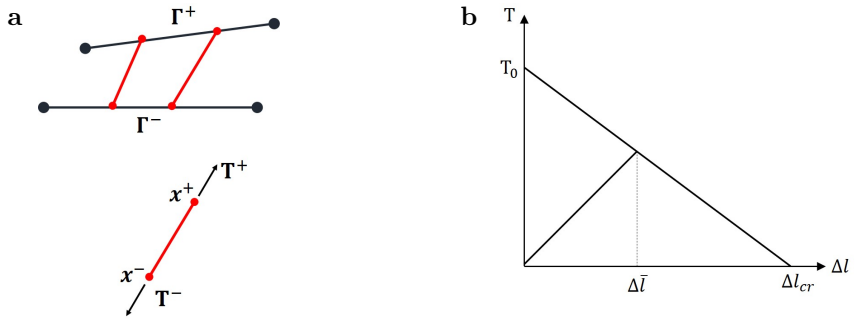

Figure 4: Large openings cohesive model: a) fibril element, b) cohesive law.

$\bar{V}(t)$ two displacement magnitudes and $f(t)$ is the time amplitude, linearly increasing in time from 0 to 1 with a total time of 1 s. Three different loading histories are considered here, namely: Case A: $\bar{U} = 0$ mm, $\bar{V} = 0.3$ mm, $c_U = 0$, $c_V = 10$; Case B: $\bar{U} = 0.15$ mm, $\bar{V} = 0.3$ mm, $c_U = 10$, $c_V = 10$; Case C: $\bar{U} = 0.5$ mm, $\bar{V} = 0$ mm, $c_U = 1$, $c_V = 0$. The adopted cohesive parameters are reported in Table 1. The numerical response obtained with the proposed procedure is compared to the those obtained by means of the small openings cohesive model and by adopting a fibril element since the beginning of the analysis. In the latter case, an elastic-softening law with fracture energy equal to G_{cr}^I and peak traction given by t_0^I is considered. The comparison is made in terms of the work of separation computed at time t as:

$$W_{coh}(t) = \int_\Gamma \int_0^{\delta(t)} \mathbf{t} d\delta \, d\Gamma \quad \text{small displacement cohesive model} \tag{41}$$

$$W_{coh}(t) = \int_\Gamma \int_0^{\Delta l(t)} \mathbf{T} d\Delta l \, d\Gamma \quad \text{fibril element} \tag{42}$$

In case A, the upper nodes of the interface are subjected to a vertical displacement of different magnitude, while in case B both horizontal and vertical displacements are applied in order to locally achieve mixed mode conditions in the small openings regime. It could be noticed from Figures 5b,5c that in both cases the numerical response computed with the proposed model initially coincides with the small openings one and then it deviates from it, as a result of the transition to the fibril model. The transition criterion is met at two subsequent time instants at the two Gauss points. Also the pure fibril model with elastic-softening behaviour is not able to catch the response predicted with the proposed model: this is due to the fact the fibril elongation at complete decohesion in the case of the insertion of the fibril element from the beginning is significantly lower than the one of the present model and that the area beneath the elastic-softening traction-separation law always coincides with the fracture energy in pure Mode I, independent of the actual mode-ratio. Moreover, both cases A and B show that the transition to the fibril element correctly accounts for the rotation and elongation of the interface's middle plane. Finally, in case C, only tangential displacements are applied, so that the fibril insertion criterion is never met and the numerical response obtained with the proposed model coincides with the one of the small openings mixed-mode cohesive model.

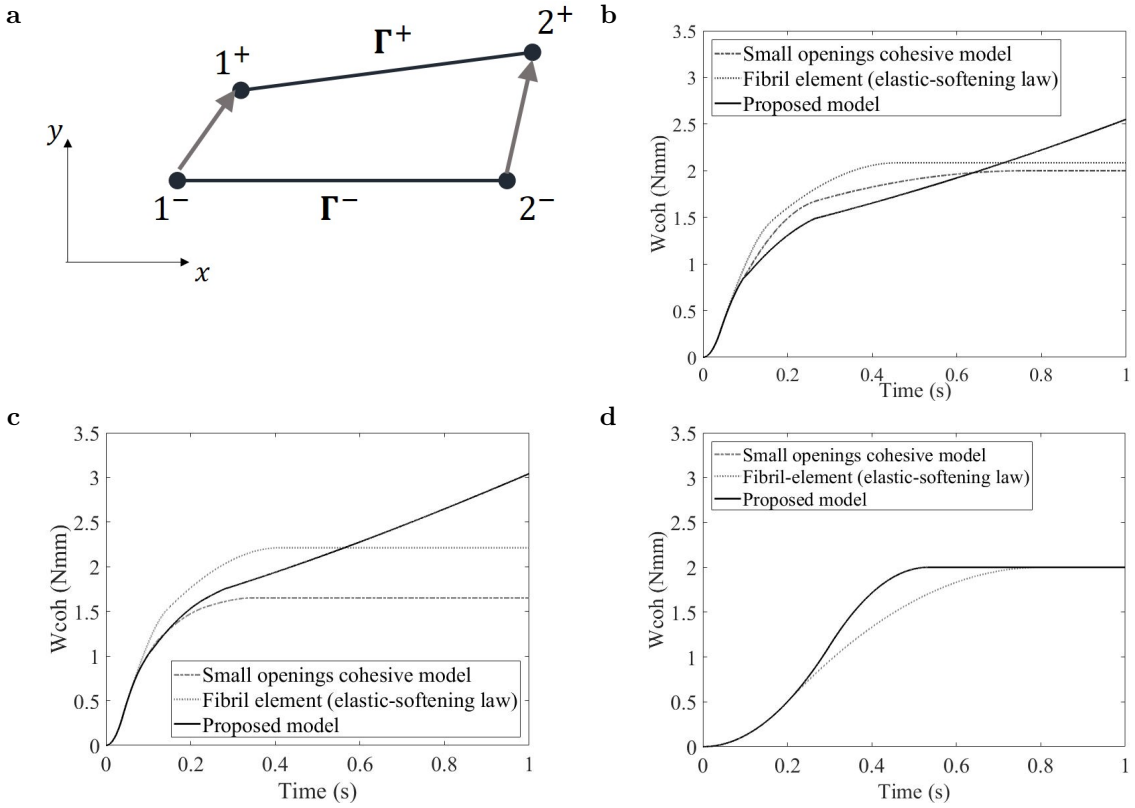

Figure 5: Numerical example: a) Interface element, b) case A, c) case B, d) case C.

t_0^I	t_i^I	t_0^{II}	G_i^I	G_{cr}^I	G_{cr}^{II}	K	α	k
10 MPa	3 MPa	15 MPa	1 $\frac{N}{mm}$	2 $\frac{N}{mm}$	2 $\frac{N}{mm}$	100 $\frac{N}{mm^3}$	30°	2

Table 1: Adopted cohesive properties.

6 CONCLUSIONS

In this work the isotropic damage cohesive model formulated in [6] under the assumption of small openings is extended to properly model both the cases of small and large openings and the presence of large-scale bridging or interfacial fibrillation. The strength of the proposed procedure is the capability to handle the transition from the small displacement case, in which the mechanical behaviour of the interface is governed by the interaction between normal and tangential openings, to the case of large openings, in which fiber bridging develops affecting the interface's response. Moreover, the adopted fibril element is able to account for large openings in a consistent way, preserving rotational equilibrium, since the interface tractions and openings are co-linear.

REFERENCES

[1] Spearing, S. M., and Evans, A.G. The role of fiber bridging in the delamination resistance of fiber-reinforced composites. *Acta metallurgica et materialia* (1992) **40**: 2191-2199.

[2] Sorensen, B. F., and Jacobsen, T. K. Large-scale bridging in composites: R-curves and bridging laws. *Composites Part A: Applied Science and Manufacturing* (1998) **29**:1443-1451.

[3] Tamuzs, V., Tarasovs, S., and Vilks, U. Progressive delamination and fiber bridging modeling in double cantilever beam composite specimens. *Engineering Fracture Mechanics* (2001). **68**: 513-525.

[4] Vossen, B. G., Schreurs, P. J. G., Van der Sluis, O., and Geers, M. G. D. On the lack of rotational equilibrium in cohesive zone elements. *Computer Methods in Applied Mechanics and Engineering* (2013) **254**: 146-153.

[5] Gilormini, P., and Diani, J. Testing some implementations of a cohesive-zone model at finite strain. *Engineering Fracture Mechanics* (2015) **148**: 97-109.

[6] Confalonieri, F., and Perego, U. Simulation of fracture and delamination in layered shells due to blade cutting. *Journal of the Serbian Society for Computational Mechanics* (2017) **11**: 139-151.

[7] Davila, C. G., Rose, C. A., and Camanho, P. P. A procedure for superposing linear cohesive laws to represent multiple damage mechanisms in the fracture of composites. *International Journal of Fracture* (2009) **158**: 211-223.

[8] Gutkin, R., Laffan, M. L., Pinho, S. T., Robinson, P., and Curtis, P. T. Modelling the R-curve effect and its specimen-dependence. *International Journal of Solids and Structures* (2011) **48**: 1767-1777.

[9] Heidari-Rarani, M., Shokrieh, M. M., and Camanho, P. P. Finite element modeling of mode I delamination growth in laminated DCB specimens with R-curve effects. *Composites Part B: Engineering* (2013) **45**: 897-903.

[10] Pagani, M., and Perego, U. Explicit dynamics simulation of blade cutting of thin elastoplastic shells using directional cohesive elements in solid-shell finite element models. *Computer Methods in Applied Mechanics and Engineering* (2015) **285**: 515-541.

[11] Confalonieri, F., Ghisi, A., and Perego, U. Blade cutting of thin walled structures by explicit dynamics finite elements. *Meccanica* (2018) **53**: 1271-1289.

[12] Van den Bosch, M. J., Schreurs, P. J. G., and Geers, M. G. D. . A cohesive zone model with a large displacement formulation accounting for interfacial fibrilation. *European Journal of Mechanics-A/Solids* (2007) **26**: 1-19.